Effects of a Novel Disulfide Bond and Engineered Electrostatic Interactions on the Thermostability of Azurin†

Anna Tigerström,‡ Frederick Schwarz,§ Göran Karlsson,⊥ Mats Ökvist,‡ Carmen Álvarez-Rúa,|| Dennis Maeder,▽ Frank T. Robb,▽ and Lennart Sjölin*,#

Department of Chemistry, Lundberg Institute, Göteborg University, Box 462, SE-405 30 Göteborg, Sweden, Center for Advanced Research in Biotechnology, National Institute of Standards and Technology, 9600 Gudelsky Drive, Rockville, Maryland 20850, Department of Molecular Biotechnology, Chalmers University of Technology, SE-412 96 Göteborg, Sweden, Departamento de Quimica Fisica y Analytica, Facultad de Quimica, Universidad de Oviedo, C/Julián Claveira 8, 33006 Oviedo, Spain, Center for Marine Biotechnology, University of Maryland Biotechnology Institute, 701 East Pratt Street, Baltimore, Maryland 21202, and Department of Chemistry and the Center for Structural Biology, Göteborg University, SE-412 96 Göteborg, Sweden

Received May 26, 2004; Revised Manuscript Received June 27, 2004

ABSTRACT: Identification and evaluation of factors important for thermostability in proteins is a growing research field with many industrial applications. This study investigates the effects of introducing a novel disulfide bond and engineered electrostatic interactions with respect to the thermostability of holo azurin from *Pseudomonas aeruginosa*. Four mutants were selected on the basis of rational design and novel temperature-dependent atomic displacement factors from crystal data collected at elevated temperatures. The atomic displacement parameters describe the molecular movement at higher temperatures. The thermostability was evaluated by optical spectroscopy as well as by differential scanning calorimetry. Although azurin has a high inherent stability, the introduction of a novel disulfide bond connecting a flexible loop with small α-helix (D62C/K74C copper-containing mutant), increased the T_m by 3.7 °C compared with the holo protein. Furthermore, three mutants were designed to introduce electrostatic interactions, K24R, D23E/K128R, and D23E/K128R/K24R. Mutant K24R stabilizes loops between two separate β-strands and D23E/K128R was selected to stabilize the C-terminus of azurin. Furthermore, D23E/K128R/K24R was selected to reflect the combination of the electrostatic interactions in D23E/K128R and K24R. The mutants involving electrostatic interactions had a minor effect on the thermostability. The crystal structures of the copper-containing mutants D62C/K74C and K24R have been determined to 1.5 and 1.8 Å resolution. In addition the crystal structure of the zinc-loaded mutant D62C/K74C has also been completed to 1.8 Å resolution. These structures support the selected design and provide valuable information for evaluating effects of the modifications on the thermostability of holo azurin.

Azurin, a copper-containing protein (MW = 14 kDa), consists of a single 128 amino acid polypeptide chain, which is folded into a Greek key barrel (*1*) consisting of one short α-helix and eight β-strands as shown in Figure 1. Azurin generally functions in an electron-transfer chain of bacteria, where it is believed to accept an electron from cytochrome c_{551} (or from the bc_1 complex) and deliver it to nitrate reductase. A recent investigation of the function of azurin from *Pseudomonas aeruginosa* indicates, however, that it not only participates in the denitrification/respiratory chain of denitrifying bacteria but also functions in response to stress situations. In particular, it has been suggested that azurin is expressed in the stationary growth phase of bacteria in response to oxidative stress (*2*).

NMR measurements show that there is an increase in the stability of azurin when the Cu^{2+}-ion in the protein is reduced to Cu^{1+}, implying that its function in the electron transfer chain is related to its conformational stability. The connection between electron transfer and protein conformation has previously been discussed for cytochrome *c* (*3*). Mutagenesis of azurin to a more stable conformation may subsequently affect its function in the electron-transfer chain. It has been demonstrated that the native disulfide bond of azurin is crucial for the stability of the protein (*4*). Since azurin is a β-sheet protein and the stability of such proteins has been studied to a lesser extent than the more prevalent α-helical or α/β proteins, it is of interest to determine the effects of mutagenesis of a β-sheet protein on its conformational stability (*5*). The azurin structure is unique in the cupredoxin family, having a disulfide bond at the N-terminus of the

† The work was supported by grants from the Swedish Natural Science Council and the Swedish Foundation for Strategic Research.
* Corresponding author. Telephone: 46+31-772 2876. Fax: 46+31-772 2853. E-mail: Sjolin@chem.gu.se.
‡ Department of Chemistry, Lundberg Institute, Göteborg University.
§ National Institute of Standards and Technology.
⊥ Chalmers University of Technology.
|| Universidad de Oviedo.
▽ University of Maryland Biotechnology Institute.
Department of Chemistry and the Center for Structural Biology, Göteborg University.

10.1021/bi048926x CCC: $27.50
Published on Web 09/09/2004

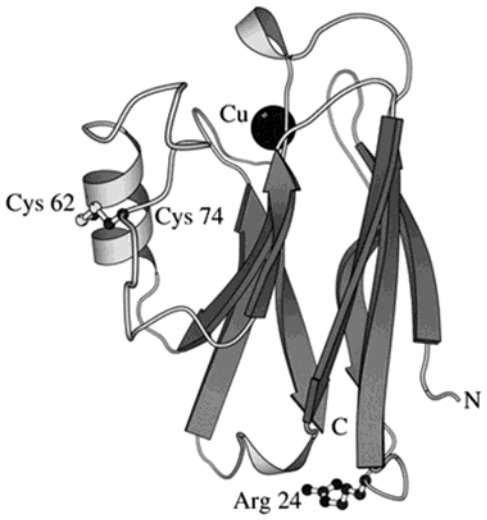

FIGURE 1: Schematic presentation of the azurin structure from *P. aeruginosa* showing its secondary structure elements. The copper ion is shown as a closed sphere and the location of the D62C/K74C and K24R mutations are in addition indicated.

protein. The phytocyanins have a disulfide bond at the C-terminus, while plastocyanin and amicyanin lack disulfide bonds. The single disulfide bond (Cys3−Cys26) in azurin is highly solvent-exposed and is located at the southern end of the protein, connecting the N-terminal ends of two β-strands. It is positioned at a distance of about 25 Å from the copper ion.

The conformational stability of azurin and a few azurin derivatives was first studied by Engeseth and McMillin (*6*), using differential scanning calorimetry (DSC).[1] These DSC studies on the thermal denaturation of azurin and its derivatives indicated the existence of two well-separated irreversible unfolding transitions for apo-azurin and only one unfolding transition for the different azurin metal derivatives. Infrared spectra of the blue copper-containing wild-type azurin and apo-azurin from *P. fluorescens* in aqueous solution (*7*) suggested that the thermal stability of the apo form is significantly reduced with respect to the native wild-type protein. Investigations of solvent isotopic effects on thermal unfolding using DSC, electron spin resonance, and optical density measurements (*8*, *9*) have shown that the thermal denaturation of azurin occurs in a rapid two-step sequence unfolding transition followed by a kinetically controlled irreversible transition.

Recently the effect of metal ligation and oxygen on the reversibility of the thermal denaturation of azurin from *Pseudomonas aeruginosa* has been deduced (*10*). The unfolding and refolding of azurin using guanidine hydrochloride (GuHCl) has also been studied by circular dichroism (CD), fluorescence, NMR, and UV using the absorption at 628 nm (*11*−*13*). Different mutants of azurin have subsequently been prepared in particular to alter the stability of the protein and have also been studied using these methods (*4*, *14*). Extrapolation of DSC scans to an infinite fast scan rate gives a transition temperature of 81.9 °C for copper-ligated wild-type azurin, indicating a very high stability for the protein. This inherently high stability of azurin presents a challenge to determine whether the protein can be further stabilized by mutagenesis.

Mutations that decrease the flexibility of the folded peptide chain at elevated temperatures also increase its stability. In this investigation, four mutations have been selected using computer-aided modeling and crystallographic information. The mutants exhibit the effects of (a) introduction of a novel disulfide bond, since disulfide bonds play a unique role in the stability of a folded protein by providing covalent cross-links between segments of the polypeptide chain, and (b) introduction of electrostatic interactions.

A recent study of a [2Fe-2S] ferredoxin from *Aquifex aeolicus* has demonstrated that the presence of a disulfide bond plays a significant role for the thermostability of the protein (*15*). Furthermore, the thermostablity of glyceraldehyde-3-phosphate dehydrogenase from the hyperthermophilic archaeon *Sulfolobus solfataricus* can be attributed to a combination of an ion pair cluster and an intrasubunit disulfide bond (*16*). Introducing a novel disulfide bond in azurin could hence further increase the thermostability of the protein. The disulfide bond selected for azurin connects a loop structure with the small α-helix (Figure 1). The disconnection of this α-helix from the main protein body could be prevented by the novel disulfide bond, and hence, the protein could be stabilized at an elevated temperature. The effects of introducing novel disulfide bonds to improve thermostability are not that straightforward. Destabilizing effects are often observed and have been attributed to the perturbation of the disulfide geometry or distortion of the local environment. Engineering of disulfide bonds into proteins is subsequently an interesting field that requires further investigations.

Introducing a favorable electrostatic interaction between two amino acid residues could also increase the thermostability of the protein (See refs *16* and *17* for discussion of this subject). The azurin mutants based on electrostatic interactions were selected to stabilize loops between two separate β strands as well as to stabilize the C-terminus (lower part of the protein in Figure 1). In terms of stability, it is possible that a separation of these loops is a crucial step at elevated temperatures. Introducing electrostatic interactions can therefore minimize separation and stabilize the protein.

Crystallographically determined temperature factors (atomic displacement parameters, ADP) at elevated temperatures according to Frauenfelder et al. (*18*) and Petsko and Ringe (*19*) were in addition used to monitor early unfolding regions in native azurin. Crystallographic studies at elevated temperatures can be carried out on protein crystals as long as they diffract X-rays. The temperature is then used to elevate the motion of protein atoms in the crystal lattice, which in turn can be measured by the atomic displacement parameters (also called Debye−Waller factors). Thus, the ADPs as determined from the normal least-squares refinement of the structure under study contain information on the dynamic motion of the protein atoms. These recalculated ADPs, determined from a difference between parameters obtained in the refinement of data from ambient temperature and elevated temperatures, contributed to the selection of the novel disulfide bond.

[1] Abbreviations: MSI, molecular structure cooperation; ADP, atomic displacement parameter; CCD, charge-coupled device; EM-MS, electron spray mass spectrometry; DSC, differential scanning calorimetry.

In this manuscript, the preparation and properties of the mutants D62C/K74C, D23E/K128R, K24R, and D23E/K128R/K24R are presented. In addition, the crystal structures of three mutants, copper-containing K24R and D62C/K74C and zinc-loaded D62C/K74C, are described.

EXPERIMENTAL PROCEDURES

1. Selection of Potentially More Stable Mutants. 1.1. Introduction of a Novel Disulfide Bond. 1.1.1. Modeling and Mutant Design. The wild-type structure of azurin from *Pseudomonas aeruginosa* was analyzed utilizing a procedure by Fersht and Serrano (*20*) to examine all possible sites in the structure for a novel disulfide bond subjected to various restraints concerning, for example, geometry. These possible sites were then engineered into the structure of azurin by computer-aided modeling using program Insight-II 2.3.5 (MSI). The wild-type azurin structure, as well as the other mutant structures, was energy-minimized after exchange of the particular amino acids.

Based on modeling of the protein structure and temperature-dependent atomic displacement parameters (see below), the novel disulfide bond was selected to connect residue 62 and 74. This disulfide bond connects a loop and an α-helix, Figure 1, and could therefore stabilize the structure at high temperatures. The temperature factors showed that residue 62 has a relatively high mobility at increased temperatures. Residue 74 on the other hand is not that mobile and could act as an "anchor" for residue 62. The double mutant, D62C/R79C, was plausible, among others, because it would introduce little distortion of the local environment compared to other disulfide bond possibilities. The site for the novel disulfide bond was also selected with respect to the already existing disulfide bond in the native protein between positions 3 and 26 to avoid problems in the folding process. A complementary investigation of the possible ion interactions in azurin showed that the mutation D62C causes the loss of the electrostatic interaction between aspartic acid 62 and arginine 79, a fact to be considered as well.

1.1.2. The Utilization of Crystallography To Monitor Movement of Amino Acids at Increased Temperatures. Temperature-dependent atomic displacement parameters (Debye−Waller factors), which describe the thermostability of proteins, were determined from X-ray data from the crystal of the wild-type azurin protein collected at stepwise increased temperatures (*21*). These data were isomorphous with data from previously reported crystals (*22*). They belong to space group $P2_12_12_1$ with cell constants $a = 57.7$, $b = 81.2$, and $c = 110.3$ Å. The crystals used in this investigation were grown from wild-type azurin protein prepared according to Karlsson et al. (*23*). One crystal of a size 0.5 mm × 0.5 mm × 0.6 mm was used for the complete data collection, and the crystal was mounted in a thin-walled glass capillary in a standard manner.

The X-ray data sets were collected on the novel SMART[2] Bruker CCD-based area detector system using molybdenum radiation. X-rays were generated using a regular sealed tube and an X-ray generator operated at 55 kV and 50 mA with a 0.4 mm × 12 mm focal spot. During the data collection, the 9 cm wide CCD detector was mounted 12.0 cm from the crystal, and the different data sets were collected at room temperature and at 28, 34, and 40 °C. One data collection attempt was done at 52 °C, but the crystal melted after only a few minutes. A graphite monochromator followed by a 0.5 mm collimator was utilized during the complete data collection. The determination of the unit cell parameters and crystal orientation and the integration of reflection intensities were performed with the SMART program system (*24*).

To measure whether the average wild-type structure was similar in the crystal at the different temperatures, an estimation of the fit between the crystal structure of the wild-type azurin model (*22*) and the X-ray data collected at each temperature was obtained. This was done by an evaluation of a linear correlation coefficient between calculated and observed structure factors. These coefficients have been widely used in macromolecular crystallography as a multipurpose tool in molecular replacement, for example, in direct rotation functions, in refinement of the model orientation, in interdomain relationships, and in translational searches (*25*, *26*).

Subsequently, the correlation coefficient between the normalized structure factors calculated from the wild-type azurin model and the X-ray data collected at different temperatures was computed using the direct rotation function, as implemented in the program X-PLOR version 3.851 (*27*). This function placed the model in a cell of P_1 symmetry with the same cell dimensions as the target crystal structure and computed a linear correlation between observed and calculated normalized structure factors in our case at a rotation angle equal to 0. Refinement of the atomic displacement parameters (ADP) was done under the consideration that the average molecular structure remained unchanged within the working range of temperatures, which was indicated from the previously calculated correlation factors.

In the beginning, the refinement of the ADPs utilized a universal atomic displacement factor for all non-hydrogen atoms in the crystal structure. This was estimated from the Wilson plot calculated on the reference data set. It was observed, however, that the starting point (use of previously refined values of isotropic ADPs or replacement of all ADPs by the universal factor) has no significant influence on the final results. The refinement of the ADPs was repeated until convergence, which was defined as when the average value of the absolute difference between the individual ADPs computed in one cycle and in the previous one was less than 0.1 Å^2 for all the C_α atoms in the crystal structure.

After convergence, the refined ADPs from each temperature interval were subtracted from the ADPs obtained in the refinement of the data set collected at room temperature. The result is presented in Figures 2 and 3. The indication of an increased instability in the non-termini region of the protein (upper part of the protein according to Figure 1) was consequently used as a base for the search of a novel disulfide bond in azurin to further stabilize the protein. The double mutant D62C/K74C was finally selected as a potentially interesting candidate.

1.2. Introduction of Electrostatic Interactions. 1.2.1. Modeling and Mutant Design. The intermonomer contact

[2] Certain commercial materials, instruments, and equipment are identified in this manuscript to specify the experimental procedure as completely as possible. In no case does such identification imply a recommendation or endorsement by the National Institute of Standards and Technology, nor does it imply that the material, instruments, or equipment identified is necessarily the best available for the purpose.

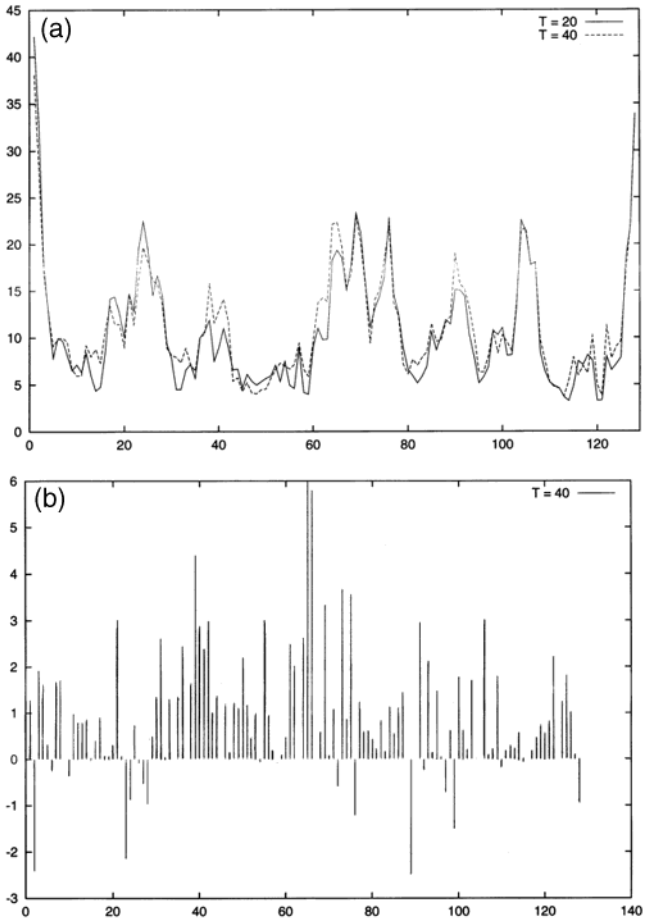

FIGURE 2: In panel a, the atomic displacement factors (ADPs) calculated as an average for the main-chain atoms are plotted as a function of the amino acid residue number based on the refinement of the wild-type azurin structure. The solid line indicates the ADPs for the structure data obtained at room temperature, while the dashed line indicates the structure data obtained at 40 °C. Panel b shows a schematic representation of the differences between the ADPs, the temperature factor data at the room-temperature subtracted from the data at 40 °C.

points are usually potential hydrogen bond formers. There are no close intermonomer ionic contacts in azurin. The intramolecular contacts are more interesting and include some stabilizing ion bridges. This part of our investigation that involves electrostatic interactions has based the ion-pair modeling on regular atomic displacement factors determined at ambient temperatures to define the more movable portions of the protein (Figure 2a). These temperature factors indicate that there is a larger thermal motion in the lower end of the β barrel where the N- and C-termini are found.

The amino-terminus has a native disulfide bridge linking Cys3 and Cys26 and should be relatively stable at higher temperatures. We suggest that loss of three-dimensional structure could start in the "south" part of the protein by degradation of the short β sheet section, followed by free movement of the C-terminus. Three mutations, K24R, D23E/K128R, and D23E/K128R/K24R, were selected on the basis of ion interactions (Figure 4). The mutants involve stabilization of this part of the protein and were selected after a thorough analysis of the structural data in this region of the protein using computer-aided modeling utilizing Insight II.

1.2.1.1. Mutant K24R. A strategy for stabilization by electrostatic interactions focuses on the amino acids in

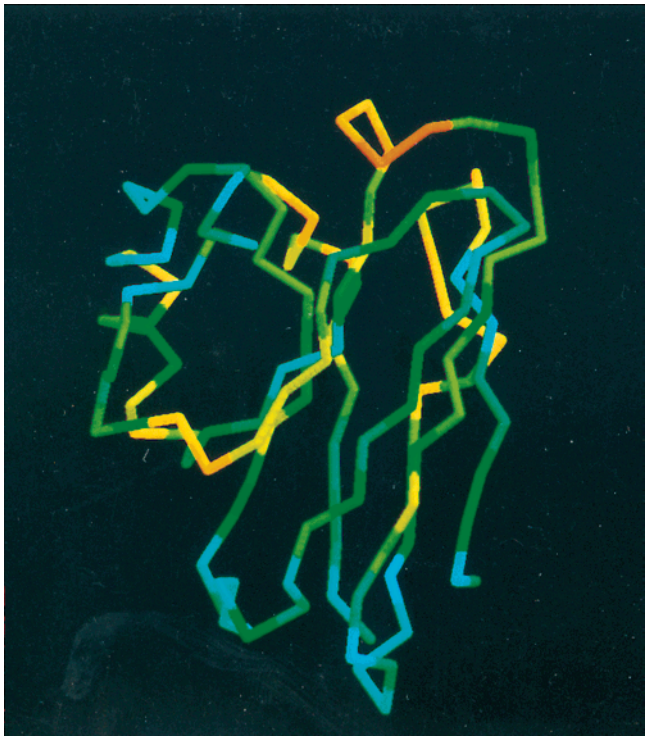

FIGURE 3: The backbone structure of azurin colored according to the novel atomic displacement parameters based on the previously described differences (red = increased motion, blue = normal motion) showing substantially increased motions in the "northern" end of the molecule.

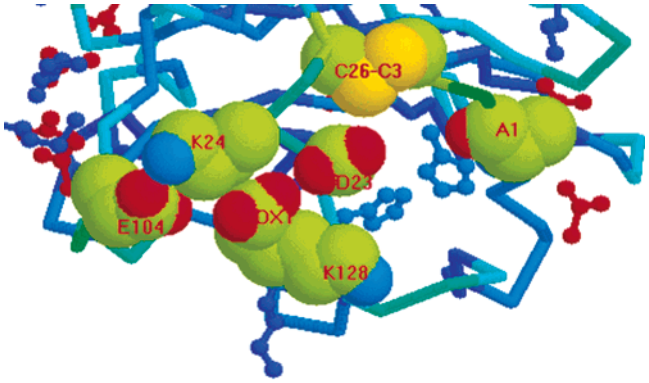

FIGURE 4: View of the termini end of the wild-type azurin structure used for the design of novel mutants with extended electrostatic interactions. The backbone is colored by utilizing regular temperature factors. Ball and stick representation of certain side chains (red = acidic and blue = basic side chains) and the space filling feature are used to view the side chains under particular analysis.

position 24 and 104. These amino acids are situated in separate loops between β-strands and are relatively close in space, see Figure 4. At high temperatures, it is possible that separation of these loops is a part of the early unfolding process. This separation can be stabilized by an electrostatic interaction. A mutation of amino acid 24 from a lysine to an arginine can make the electrostatic interaction between position 24 and 104 more favorable. The delocalization of the positive charge in arginine gives many microstates and more possibilities for an electrostatic interaction to be formed also at higher temperatures when the amino acids are having more motions in general. The mutation can also make the distance of the electrostatic interaction shorter and more favorable. In terms of stability, it is possible that separation

of the two loops is a crucial step at elevated temperatures, but the area could be stabilized by K24R. However, the mutation can also affect the electrostatic interaction between K24 and K128, and this must be considered when evaluating the results.

1.2.1.2 Mutant D23E/K128R. In the native state, amino acid 23 is an aspartic acid and located in a loop, according to Figure 4. The carboxyl group of this amino acid is relatively near in space to the α-carboxyl group of amino acid 128. One way to stabilize the C-terminal end is therefore to decrease the repulsion between the negative charges from amino acid 23 and 128. A useful strategy would be to displace the aspartic acid with glutamic acid. Since glutamic acid is one CH_2-group longer compared to aspartic acid, this carboxyl group from amino acid 23 is moved further away from the α-carboxyl group of amino acid 128. A combination of this mutation, D23E, with a displacement of the native lysine in position 128 to an arginine, K128R, could produce a favorable electrostatic interaction between glutamic acid in position 23 and arginine in position 128. The extra delocalized ionic pair interaction and a more favorable distance could hence stabilize the mutant. Furthermore, residue 23 is relatively closely located in space to residue 26, which is covalently bonded to residue 3 by the native disulfide bond and hereby stabilized. The described strategy can be a way of stabilizing amino acid 128 and the C-terminal end.

Investigation of possible electrostatic interactions in azurin further reveals that the mutation D23E can affect the electrostatic interaction between amino acid D23 and T126 and the mutation K128R can affect the corresponding interaction between K128 and V22 and the interaction between K128 and K24. These are factors are to be considered when evaluating the effects of this double mutant with respect to thermostability.

1.2.1.3. Mutant D23E/128R/K24R. By a combination of the above-described effects from mutant D23E/K128R and K24R, this triple mutant reflects the additive effect of electrostatic interactions on thermostability. These mutations involve stabilization of the C-terminal end, as well as the stabilization of loops between two β-strands.

2. Site-Directed Mutagenesis, Expression, and Purification. The QuickChangeTM site-directed mutagenesis kit was used to introduce select mutations. The mutants were sequenced with Automated Laser Fluorescence DNA Sequencer from Pharmacia. Azurin was expressed in *Escherichia coli*, and the purification of the protein was performed as previously described by Karlsson et al. (*23*). Purification involved periplasmic preparation using a 20% sucrose solution and subsequent osmotic chock as the cells were transferred to a 0.5 mM $MgCl_2$ solution. $CuSO_4$ was added to the protein solution and taken up by azurin. Further purification involved pH precipitation with 0.5 M ammonium acetate, pH 4.1, and cation-exchange chromatography with a pH gradient of 4.1 to 9.0, followed by size-exclusion chromatography. Copper-containing mutants proven to have an increased stability in the DSC measurements were also expressed, purified, and analyzed in the corresponding zinc form for further investigation. Zinc-loaded derivates were cultivated in media containing 100 μM $ZnSO_4$.

3. Verification of the Mutations. In addition to DNA sequencing the mutant proteins were further verified by mass spectrometry (MS) and electron spray mass spectrometry (EM-MS). MS and EM-MS were performed on a hybrid quadropole-orthogonal acceleration time-of-flight mass spectrometer (Micromass UK, Ltd., Wythenshave, Manchester, U.K.) equipped with a nanoflow electrospray probe. The nanoflow source was operated at a temperature of 30 °C with a nitrogen drying gas flow of 40 L h^{-1}. A potential of 1.0−1.4 kV was applied to the nanoflow tip, and a nitrogen back pressure of 5−6 psi produced a flow rate of about 10−30 nL min^{-1}. Data were acquired in continuum mode with an integration time of 10 s. Ellman's reagent was used to verify the absence of free cysteines, compared to the wild-type, in the mutant with the novel disulfide bond.

4. Thermostability Measurements by Spectrophotometry. UV−visible spectra were recorded on a Cary 4.0 spectrophotometer. Thermal denaturation experiments were performed on mutants containing Cu^{2+} ions in the metal site. The temperature was scanned at 0.3 °C min^{-1} in 10 mM phosphate buffer, pH 7.0, at a protein concentration of 1 mM using the wavelength of 628 nm. The temperature scan ranged from 25 to 90 °C. The optical measurements were performed in 1 mL quartz cuvettes. The T_m values were recorded at the temperature where the transition curve exhibits a maximum in its slope. The A_{628}/A_{280} absorption ratio was in addition estimated at room temperature (20 °C).

5. Thermostability Measurements by Differential Scanning Calorimetry. DSC measurements were performed by using a VP-DSC microcalorimeter from Microcal, Inc. (Northampton, MA). The DSC consists of a matched pair of 0.511 mL sample and reference vessels. In a series of DSC scans at a set scan rate, both vessels were first loaded with buffer solution (100 mM potassium phosphate, pH 7.0), equilibrated at 20 °C for 15 min, and scanned up to 90 °C at the preset scan rate (30, 45, 60, or 90 °C h^{-1}). The buffer versus buffer scan was repeated once, and upon the second cooling, the sample vessel was emptied, rinsed several times, and loaded with the protein solution by means of a syringe prior to the 15 min equilibration period at 15 °C. This procedure was repeated with the other protein solutions after each solution was scanned twice to determine whether the transition was reversible. For the scans run under oxygen-free conditions, the solution from the previous scan was removed, and the sample cell was washed with buffer and then purged with dry nitrogen prior to injection of the deaerated sample solution. Deaeration of the solutions was achieved by stirring of the solutions under vacuum. The protein solutions were from 0.1 to 5 mM, and care was taken to minimize the presence of air bubbles in the loading of the sample vessel. After completion of a set of scans, the second buffer vs buffer scan was used as the baseline scan and subtracted from each of the protein solution vs buffer scans prior to analysis. The net solution versus buffer scan was analyzed by using the EXAM software program (*28*) to determine the transition peak area and the temperature where the transition peak is a maximum at each of the scan rates. A sigmoidal baseline, which followed the profile of the transition peak, was used to extrapolate the pre- and posttransitional baselines under the transition peak in the determination of the transition peak area. For the transitions that are irreversible in the oxidized state of the protein and depend on scan rate, thermodynamic equilibrium two-state transition models cannot be applied to the analysis of the data. Therefore only the transition peak

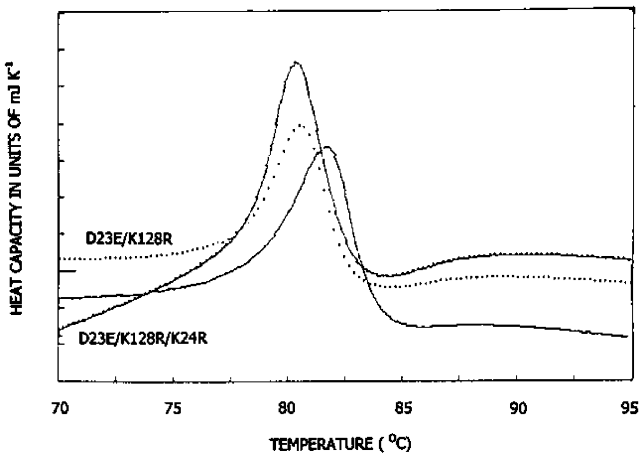

FIGURE 5: Comparison of the DSC scans of the Cu-D23E/K128R mutant (broken curve) and the D23E/K128R/K24R mutant (solid curve) to that of azurin (solid, lower transition peak). The samples were 1 mg mL^{-1}, the sample size was 0.511 mL, and the scan rate was 80 °C h^{-1}.

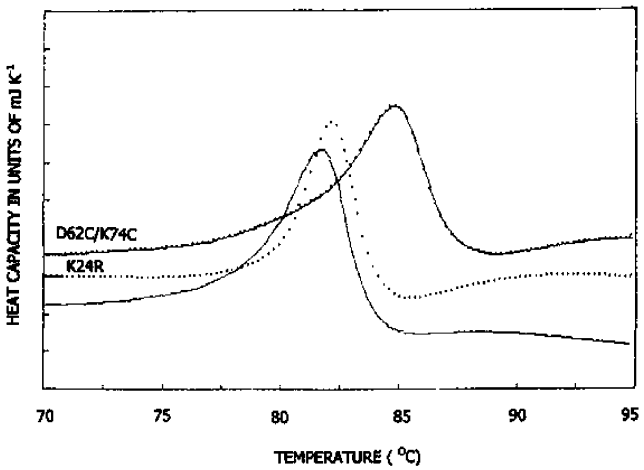

FIGURE 6: Comparison of the DSC scans of the Cu-K24R mutant (broken curve) and the D62C/K74C mutant (solid curve) to that of azurin (solid, lower transition peak). The samples were 1 mg mL^{-1}, the sample size was 0.511 mL, and the scan rate was 80 °C h^{-1}.

area per mole of protein ($\Delta_{trs}H$) and the temperature at the peak maximum, T_m, were recorded at each scan rate (cf. Figures 5 and 6). For Zn mutant transitions that are reversible, the EXAM program also yielded the van't Hoff enthalpy ($\Delta_{trs}H_{vH}$) from the shape of the transition peak. The ratio of the enthalpies yields the cooperativity of the transition. For a two-state A ⇔ B transition without any intermediate states, the ratio is 1.

6. Crystallization, Data Collection, and Data Processing. Crystals from the two copper-containing azurin mutants, K24R and D62C/K74C, as well as zinc-containing mutant D62C/K74C, were obtained. The crystals were grown by the hanging-drop vapor-diffusion method. The crystallization experiments for the copper-containing mutants were carried out at room temperature, and the most successful conditions utilized 20−23% PEG 3350, 0.25 M $MgCl_2$, and 0.1 M sodium acetate buffer at pH 4.5. The drops consisted of a mixture of 2 μL of reservoir and 2 μL of protein solution. Elongated crystals appeared for the K24R mutant within 2 days and grew to maximal dimensions of about 0.8 mm × 0.3 mm × 0.2 mm. The crystals from mutant D62C/K74C also appeared after a few days and grew to a maximal size of 0.7 mm × 0.2 mm × 0.2 mm. The color of the crystals from both mutants was deep blue, consistent with the copper ion being in the oxidized form (Cu^{2+}). Elongated or prismatic transparent crystals from Zn-D62C/K74C were obtained from a mixture of 0.2 M ammonium sulfate, 0.1 M cacodylate at pH 6.5, and 30% PEG 8000 using mixture of 1 μL of reservoir and 1 μL of protein solution. However they took ca. 14 days to grow to a maximum size of about 0.8 mm in the longest direction.

An X-ray diffraction data set to a resolution of 1.8 Å was collected for the K24R mutant on beam-line I711 at the synchrotron in Lund (Max Lab II). In preparation for the synchrotron radiation data collection, the azurin crystals were transferred briefly to a cryoprotectant solution containing 25% PEG 400 in addition to the mother liquor before flash freezing in the cryogenic nitrogen gas stream (100 K). X-ray diffraction data from a total rotation of 200° were collected in steps of 0.2° from one crystal. The crystal-to-detector distance was 140.0 mm, and the wavelength was 0.991 Å. These data were integrated using the program XDS and scaled and merged using XSCALE (*29*). The final data set after internal scaling consisted of 20 500 independent reflections to 1.8 Å resolution, and the data set represents 99.2% of the expected number of reflections to this resolution. The redundancy of the data was 11-fold, and the average $I/\sigma(I)$ was 53.5. The estimated temperature factor from Wilson scaling was 19.0.

A data set for the Cu-D62C/K74C mutant to 1.5 Å resolution was later collected at the same beamline, using the same cryo conditions. A total of 200° of rotation data were collected in 0.5° steps with the detector 130.0 mm from the crystal and with the wavelength of 1.095 Å. This data set was processed and scaled using XSCALE (*29*). The final data set after internal scaling consisted of 34 706 reflections to 1.5 Å resolution, and the data set represents 99.6% of the expected number of reflections to this resolution. The redundancy of the data was 6-fold, and the average $I/\sigma(I)$ was 26.3. The estimated temperature factor from the Wilson scaling procedure became 17.2.

Finally a data set for the Zn-D62C/K74C mutant to 1.8 Å resolution was collected under cryo conditions on the in-house Oxford Diffraction Xcalibur CCD system. The data were processed and subjected to geometric corrections and internal scaling using the MOSFILM and SCALA programs. A total of 23 540 reflections representing 97.4% completion and with a redundancy factor of 4.0 were analyzed with Wilson statistics, and the overall temperature factor became 18.8.

7. Structure Solution and Refinement. The K24R mutant structure was solved by molecular replacement using the wild-type azurin structure as a search model (PDB ID, 4AZU). The solvent molecules and the copper atom were removed from the search model before the structure was determined utilizing the molecular replacement technique in AMORE (*30*) of the CCP4 4.1 suite (*31*). Rotation and translation functions clearly identified two independent solutions. After rigid body refinement using REFMAC5 (*32*), this solution yielded an *R*-factor of 43.5% (R_{free} = 44.7%). The model was then subjected to two rounds of simulated annealing (torsion angle molecular dynamics) starting at 4000 K and in addition energy minimization using CNS (*33*) to minimize model bias. Subsequent refinement was carried out

Table 1: Data Collection Statistics and Refinement Results from the Structure Solution of the D62C/K74C(Cu), D62C/K74C(Zn), and K24R(Cu) Mutants

dataset:	D62C/K74C(Cu)	D62C/K74C(Zn)	K24R(Cu)
temperature (K)	100	100	100
	Unit Cell Constants		
a (Å)	81.4	113.1	41.2
b (Å)	87.3	50.0	65.0
c (Å)	31.4	57.7	88.0
β (deg)	90.0	119.5	90.0
space group	$P2_12_12$	$C2$	$P2_12_12_1$
crystal mosaicity	0.54	0.61	0.48
	No. of Measurements		
unique reflns	34 706	23 540	20 500
data completeness	99.6	97.3	99.2
R_{merge}[a]	7.3%	6.5%	5.2%
no. of atoms	2224	1991	2076
protein atoms	1923	1925	1927
ligand atoms (Cu/Zn)	2	2	2
solvent atoms	299	101	147
	rms Deviations		
bond lengths (Å)	0.020	0.016	0.013
bond angles (deg)	1.670	1.473	1.345
resolution range	59.8−1.5	50.3−1.8	52.0−1.8
R value[b] (%)	19.7	19.3	17.2
R_{free} (%)	23.6	23.8	21.9

[a] $R_{merge} = \sum_H \sum_{i=1}^{N} |\langle I(H)_i \rangle - I(H)_i| / \sum_H \sum_{i=1}^{N} I(H)_i\}$ where $I(H)_i$ is the *i*th measurement of reflection *H*, $\langle I(H)_i \rangle$ is its mean value, and the summation extends over all the reflections measured more than once in the set. [b] $R = \sum |F_o - F_c| / \sum |F_o|$.

using REFMAC5. After 22 rounds of refinement and intervening model building using the molecular graphics program O (*34*), the two peptide chains consisted of 1927 protein atoms, 2 copper atoms, and 147 solvent molecules. In the final round of refinement, the R_{free} value reached 21.9% with a conventional *R* of 17.2%.

The structure solution for the Cu-D62C/K74C mutant was started from the dimer obtained as a molecular replacement solution from AMORE for the K24R mutant but with the amino acids in the 62 and 74 positions replaced with alanine residues. After rigid body refinement, the structure was further refined in two rounds of simulated annealing beginning at 6000 K (*33*). After 10 rounds of subsequent energy minimization and intervening manual rebuilding using the program O operating on electron density maps calculated from the data, the *R*-factor became 19.2% and R_{free} 21.8%. The final model consists of 1923 protein atoms, 2 copper atoms, and 299 solvent molecules.

Similarly the structure solution for the Zn-D62C/K74C mutant was started using the wild-type azurin structure as a search model (PDB ID, 4AZU) but with the amino acids in the 62 and 74 positions replaced with alanine residues. The continued procedure followed closely the previously described protocol for the K24R mutant leading to a final dimeric model consisting of 1925 protein atoms, 2 zinc atoms, and 101 solvent molecules to a resolution of 1.8 Å. The final *R*-factor became 19.3% and R_{free} 23.8%.

The results and the statistics obtained from the data collection and refinement procedure of these three azurin mutants are presented in Table 1. The coordinates for the three structures have been deposited at the protein data bank, PDB reference codes: 1XB3, 1XB6, and 1XB8.

Table 2: Molecular Mass Measured by Mass Spectrometry for Azurin and the Mutants[a]

mutant	molecular mass, g mol^{-1}	measured difference, g mol^{-1}	calculated difference, g mol^{-1}
wild-type	14 005.57		
D23E/K128R	14 046.72	+41.15	+42.03
K24R	14 032.29	+26.72	+28.01
D23E/K128R/K24R	14 074.33	+68.76	+70.04
D62C/K74C	13 966.50	−39.07	−38.98

[a] The differences in mass between the mutants and the wild-type protein is indicated.

RESULTS

Verification of the Mutants. The selected mutants were verified by mass spectrometry, as well as automated laser fluorescens (ALF) sequencing. The molecular masses for the mutants and the wild-type azurin protein obtained by the mass spectrometry measurements are presented in Table 2. The expected differences between the wild-type protein and the mutants, calculated on the basis of the molecular mass for the wild-type and the mass of the introduced amino acids, are also presented in Table 2. The measured differences compared to the calculated ones agree in general within one mass unit. The use of Ellman"s reagent showed that no free cysteines were present in the D62C/K74C mutant compared to the wild-type protein as a consequence of the novel disulfide bond (not shown).

Thermostability Measurements by DSC and Spectrophotometry. Typical DSC scans on azurin and the mutants (all containing copper) are shown in Figures 5 and 6. The DSC scans of the D23E/K128R and D23E/K128R/K24R mutants in Figure 5 show that they begin to denature at a lower temperature than the wild-type azurin protein, while the K24R and D62C/K74C mutants begin to unfold at a higher temperature than azurin (Figure 6).

All the transitions exhibit a shallow exotherm at the high temperature limit of the transition peak. The transition peaks did not reappear upon cooling the samples and subsequently rescanning the samples, indicating that the transitions are irreversible. The maximum peak temperatures and peak areas are presented in Table 3 for azurin and the mutants. Since, as shown in Table 3, the transition enthalpy and temperature are dependent on the scan rate, the thermal denaturation of azurin and mutants is kinetically controlled, as well as being irreversible, and thus cannot be analyzed in terms of a thermodynamic model. Instead, they were analyzed in terms of a kinetically controlled thermal denaturation transition using the methods first described by Sanchez-Ruiz et al. (*35*) and later applied to azurin by La Rosa et al. (*8*) and to the C3A/C26A azurin mutant by Guzzi et al. (*9*). This method involves determining an apparent activation energy for the thermal denaturation, which is dependent on the reversible unfolding enthalpy of the protein, $\Delta_{trs}H_u$, and the energies of the kinetically controlled processes as shown,

$$E_{app} = \Delta_{trs}H_u + \Delta_{act}E + \Delta_{agg}H \qquad (1)$$

where $\Delta_{act}E$ is the activation energy for the irreversible transition of the unfolded protein and $\Delta_{agg}H$ is the enthalpy for irreversible aggregation of the unfolded protein. Values for $\Delta_{trs}H_u$ and the transition temperature for azurin and each

Table 3: Thermodynamic Parameters of Copper-Containing Azurin and Mutants Obtained from DSC at Different Scan Rates[a]

	20 °C h^{-1}		40 °C h^{-1}		60 °C h^{-1}		80 °C h^{-1}		∞ °C h^{-1}	
mutant	T_m (°C)	$\Delta_{trs}H$ (kJ mol^{-1})	T_m (°C)	$\Delta_{trs}H$ (kJ mol^{-1})	T_m (°C)	$\Delta_{trs}H$ (kJ mol^{-1})	T_m (°C)	$\Delta_{trs}H$ (kJ mol^{-1})	T_m (°C)	E_{app} (kJ mol^{-1})
wild-type	78.7	590	80.0	560	81.0	542	81.6	568	81.9	473 ± 23
D23E/K128R	78.0	373	79.0	450	79.9	512	80.5	303	81.0	541 ± 30
K24R	79.5	858	80.8	519	81.6	627	82.4	316	82.9	498 ± 28
D23E/K128R/K24R	77.8	439	79.1	720	79.8	505	80.5	488	81.0	547 ± 14
D62C/K74C	81.4	928	83.0	542	83.6	515	85.2	304	85.6	388 ± 39

[a] Uncertainty in the temperatures is 0.1 °C, and uncertainty in the $\Delta_{trs}H$ values is 8%.

mutant can be obtained by extrapolation of the DSC results to infinite scan rate, where contributions from the slower kinetically controlled process are negligible. Attempts to determine $\Delta_{trs}H_u$ and the transition temperature using the extrapolation procedure described by La Rosa et al. (*8*) were unsuccessful, however, since accurate extrapolation of the exponential dependence of $\Delta_{trs}H_u$ and transition temperature on the scan rate would require more than just the four scan rates used in these DSC measurements. It should be emphasized, however, that the T_m values at every scan rate in Table 3 are always in the following order: D62C/K74C > K24R > wild-type > D23E/K128R = D23E/K128R/K24R. This would imply that the thermal stabilities are in the same order. If the T_m values in Table 3 are plotted as a function of υ^{-1}, where υ is the scan rate in °C min^{-1}, the dependence appears to be linear. At infinite scan rate where $\upsilon^{-1} \rightarrow 0$, values for T_m were obtained and are presented in Table 3 to further illustrate this implication.

Values for the apparent activation energy (E_{app}) for the thermal denaturation transition were obtained by using the equation

$$\ln(\upsilon/T_m^2) = C - (E_{app}/(RT_m)) \quad (2)$$

where $R = 8.315$ J mol^{-1} K^{-1} and C is a constant in the experiment. Values for E_{app} were calculated from the slope of the linear plot of $\ln(\upsilon/T_m^2)$ versus $1/T_m$ and are presented in Table 3. They range from 388 kJ mol^{-1} for D26C/K74C to 547 kJ mol^{-1} for D23E/K128R/K24R. In the case of wild-type azurin, it was 473 ± 23 kJ mol^{-1}, in good agreement with 451 kJ mol^{-1} obtained by UV melting temperature analysis on azurin (*7*). Since higher transition temperatures indicate higher values for $\Delta_{trs}H_u$, a comparison of the transition temperatures with the apparent activation energies in Table 3 indicate that contribution from $\Delta_{act}E$ and $\Delta_{agg}H$ in eq 1 become more exothermic as the stability of the mutant increases. This was also observed for the C3A/C26A where a transition temperature of 64.72 ± 0.06 °C, $\Delta_{trs}H_u$ of 444 ± 18 kJ mol^{-1}, and E_{app} of 508 kJ mol^{-1} were obtained by extrapolation. The reason for this correlation is not known.

DSC scans of the deaerated solutions of the Zn-K24R mutant exhibited reversibility since the transition peak reappeared upon a rescan of the solution as shown in Figure 7. Values for the transition parameters from the fit shown in Figure 7 are presented in Table 4. If the solution were scanned without prior deaeration of the sample, a transition peak would appear only in the first scan of the sample, although the transition temperatures and enthalpies were close to those determined from an analysis of the deaerated sample transition peak (Table 4). The results shown in Table 4 were from scans performed at the fastest scan rate to minimize high-temperature degradation of the unfolded protein and to minimize the amount of air diffusing into the sample. For example, for DSC scans of the K24R mutant performed at a slower scan of 18 °C h^{-1}, the transition peak area of the repeat scan was 5% of that of the first scan, while at 90 °C h^{-1}, the transition peak area of the repeat scan was 50% of that of the first scan. The A_{628}/A_{280} absorption ratio for this mutant was set to 0.0 since no detectable A_{628} peak was obtained from the spectroscopic measurements

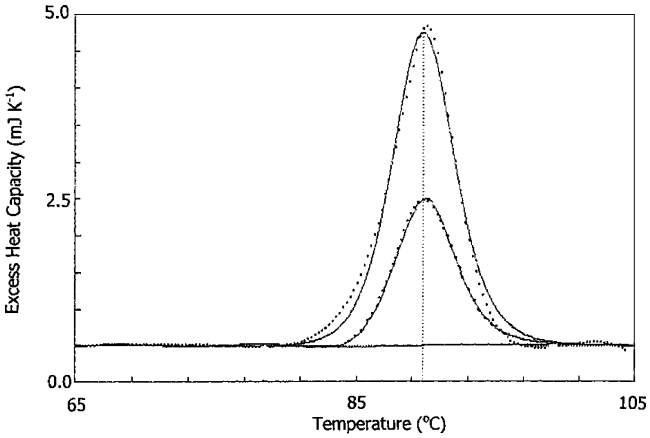

FIGURE 7: Results of a DSC scan of a deaerated 0.085 mM Zn-K24R mutant solution. The smaller transition profile is the result of a repeat scan of the sample. The sample size was 0.511 mL, and the scan rate was 90 °C h^{-1}. The solid lines are fits of a two-state transition model to the data that are indicated by the broken line.

Table 4: Thermodynamic Parameters of the Thermal Unfolding of the Zinc Wild-Type and Mutant Derivatives from DSC Scans Performed at 90 °C h^{-1}

azurin derivative	T_m (°C)	$\Delta_{trs}H$ (kJ mol^{-1})	$\Delta_{trs}H_{vH}$ (kJ mol^{-1})	enthalpy ratio
Zn(II) wild-type[a]	89.6 ± 0.1	660 ± 28	765 ± 23	1.16 ± 0.06
repeat scan[a]	89.8 ± 0.1		786 ± 24	
Zn(II)K24R	90.7 ± 0.1	600 ± 30	757 ± 38	1.26 ± 0.09
repeat scan	90.5 ± 0.1		766 ± 38	
Zn(II)K24R	89.9 ± 0.1	591 ± 30	627 ± 33	1.06 ± 0.07
D62C/K74C	88.6 ± 0.1 and 92.6 ± 0.1		555 and 1061	
repeat scan	85.7 ± 0.1		961	
D62C/K74C	88.0	505	852	1.68 ± 0.12

[a] Scans were performed at 80 °C h^{-1}, and the results are from ref *10*.

DSC scans of deaerated solutions of the Zn-D62C/K74C mutant exhibited a broad transition at 90 °C, which could be resolved into a two-state transition at 88.6 °C and a smaller two-state transition (15% of the total broad peak area) at 92.6 °C (Figure 8a,b). There is also a small transition peak at 65 °C (not shown in figures) that is observed only in the

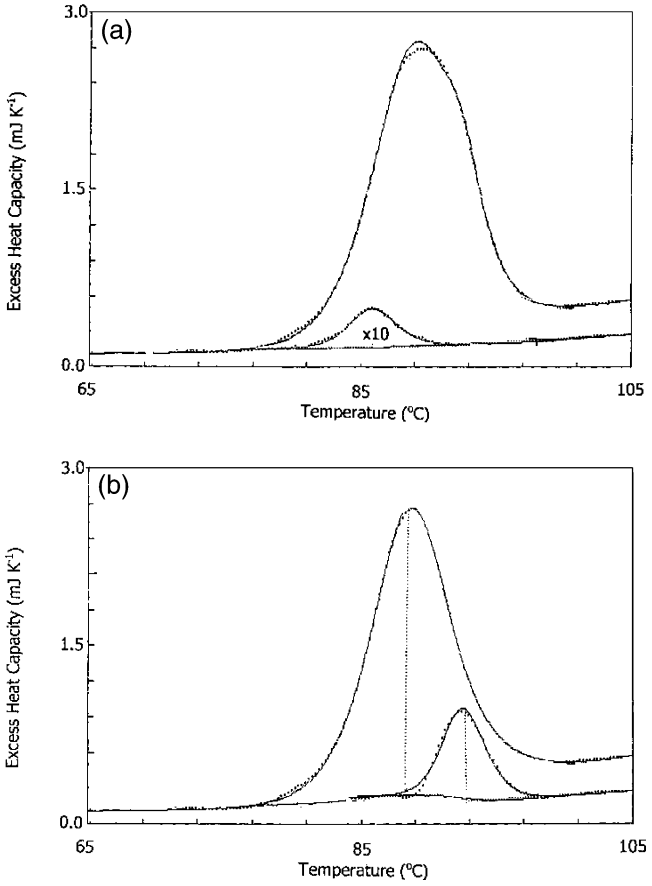

FIGURE 8: Panel a shows the results of a DSC scan of a deaerated 0.07 mM Zn-D62C/K74C disulfide mutant solution. The smaller transition profile is the result of a repeat scan of the sample. The sample size was 0.511 mL, and the scan rate was 90 °C h^{-1}. The solid lines are fits of a two-state transition model to the data that are indicated by the broken lines. The solid line fit for the initial larger transition was performed by resolving this broad transition peak into the two transitions shown in panel b. Panel b shows the two transitions that were obtained by resolution of the initial broad transition peak exhibited by the DSC scan of the deaerated 0.07 mM Zn disulfite mutant shown in panel a. The solid lines are the fits of each transition to a two-state transition model. The vertical lines are at the transition temperature.

first scan of the D26C/K74C solution. Upon a rescan of the solution, partial reversibility of the broad transition peak at 90 °C was confirmed by the appearance of a smaller transition peak with a maximum shifted to 86 °C and an area equal to 6.7% of the original broad transition. Interestingly, the initial DSC scan of the D62C/K74C mutant solution is almost identical to that of the apo-azurin at a molar ratio of 0.3 Cu^{2+} to protein in Engeseth et al. (*6*). At a molar ratio of 0.3 Cu^{2+} to protein, a small transition peak is observed at 60 °C and a broad apparently merged double transition peak is observed around 85 °C. However, the crystal structure of this mutant unambiguously indicates that the zinc metal site is fully occupied within the experimental precision, and the reason for the two-state transition probably stems from the introduction of the novel disulfide in the structure. The measured A_{628}/A_{280} absorption ratio of 0.03 indicates that a very low amount of Cu^{2+} is found in the D62C/K74C mutant solution.

The thermal denaturation of copper-containing azurin and the mutants was also followed by light absorption measurements at 628 nm with a standard spectrophotometer, and the

Table 5: Spectrophotometry Results on the Wild-Type Azurin and Mutants

mutant	T_m (°C)
wild-type	78 ± 1
D23E/K128R	74 ± 1
K24R	76 ± 1
D23E/K128R/K24R	75 ± 1
D62C/K74C	78 ± 1

T_m values are presented in Table 5. The T_m results show almost the same order of stability with, however, the wild-type (T_m = 78 °C) as stable as the D62C/K74C mutant (78 °C) and more stable than the K24R mutant (76 °C). It is important to notice that the light absorption measurements only reflect the local stability of the area around the copper ion while calorimetric investigations determine global changes in the stability. The near-constant ratio of the optical density at 280 nm where only the protein absorbs light to that at 628 nm where the ligated copper absorbs light indicates that the mutations have little effect on the structure around the copper ion.

The Crystal Structure of Mutants D62C/K74C (Cu- and Zn-Loaded) and Cu-K24R. The three crystal structures to 1.5, 1.8, and 1.8 Å resolution, respectively, refined to final crystallographic *R*-values of 19.7%, 19.3%, and 17.2%. The quality of the structure solutions is indicated in Figure 9a,b, where regular $2F_o - F_c$ maps are utilized to show the primary electron densities obtained at the mutation sites. The three mutant structures were in addition superposed on the azurin wild-type structure using the C_α positions as targets, successively decreasing the cutoff distance down to 0.3 Å to exclude atoms from the fitting process. The rmsd's calculated on the backbone atoms became 0.20−0.30 Å.

Figure 10 shows the result of the superposition of Cu-D62C/K74C onto the wild-type structure, and it is clearly indicated in the figure that there are only small differences between the structures mainly found in the loop regions. In the K24R structure, the loop region including residue 104 in which new hydrogen bonds have been formed with Arg24 has become more stabilized as judged from the electron density maps and the temperature factors compared to the other wild-type and mutant structures. An inspection of the copper sites in the two mutants reveals that these areas are very similar to the wild-type structure as can be seen from Table 6. The zinc position in the Zn-D62C/K74C mutant is also very close to the previously determined zinc position in the zinc-loaded wild-type azurin structure.

DISCUSSION

1. Introduction of a Novel Disulfide Bond. 1.1. X-ray Crystallography at Elevated Temperatures as a Tool for Mutant Design. Vital support for the two selected amino acids was given by the utilization of the novel atomic displacement factors described above. Generally, crystallographic studies at elevated temperatures can be carried out on protein crystals as long as they diffract X-rays. The temperature is then used to increase the motion of protein atoms in the crystal lattice, and that in turn can be described by regular atomic displacement factors (ADP). Thus, the ADPs as determined from the normal least-squares refinement of the structure under study contain information on the

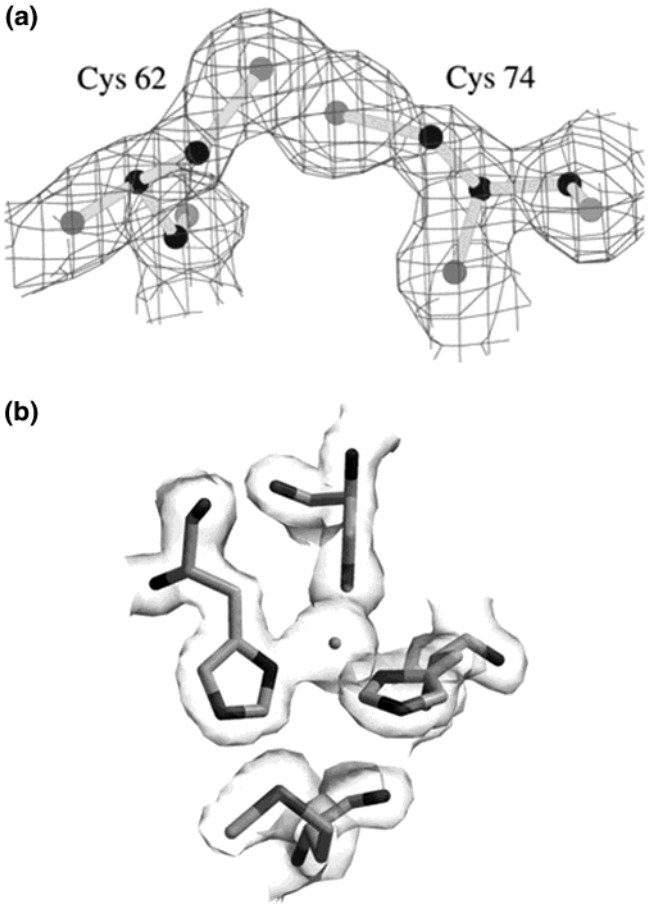

FIGURE 9: Panel a shows the electron density $2F_o - F_c$ omit map covering the engineered disulfide bridge D62C/K74C. Panel b shows the Zn metal site in the Zn-D62C/K74C mutant presented with the covering electron density obtained from a $2F_o - F_c$ omit map. The position of the Zn ion and its ligands are in addition indicated. The focus is on the short distances between the zinc ion and His46, His117, and Cys112. In addition, the long distance to Met121 is also clearly seen.

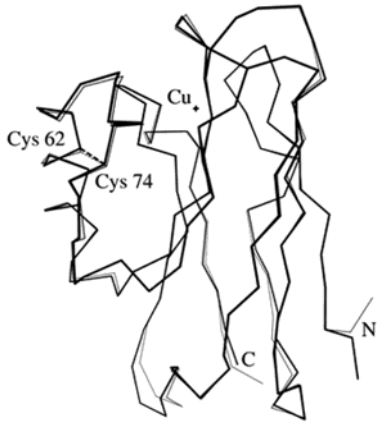

FIGURE 10: Superposition of the wild-type azurin structure from *Pseudomonas aeruginosa* (*1*) and the Cu-D62C/K74C mutant structure.

dynamic motion of the protein atoms. In addition, these factors contain information on thermal vibrations, static disorder, and lattice disorder, all contributing to the magnitudes of these parameters.

These novel atomic displacement factors, calculated from a series of X-ray data from crystalline wild-type azurin, indicated that residue 62 has a relatively high mobility at elevated temperatures (cf. Figure 2), while residue 74 is not that mobile and may therefore act as an "anchor" for residue 62. This suggestion highly contributed to the final selection of a novel disulfide, and subsequently the D62C/K74C mutant was constructed.

Table 6: The Metal Site Geometry in the D62C/K74C and K24R Mutants[a]

	D62C/K74C subunit		K24R subunit		
bond	I	II	I	II	wild-type
Cu−O (45)	2.73	2.81	2.81	2.81	2.87
Cu−Nd1 (46)	2.04	2.04	2.11	2.13	2.11
Cu−Nd1 (117)	2.02	2.00	2.07	2.13	2.03
Cu−Sg (112)	2.25	2.21	2.21	2.23	2.25
Cu−Sd (121)	3.31	3.27	3.28	3.25	3.25
Zn−O (45)	2.17	2.20			
Zn−Nd1 (46)	2.14	2.15			
Zn−Nd1 (117)	2.12	2.19			
Zn−Sg (112)	2.25	2.27			

[a] The metal−ligand bond length is given in Å units, and the number of the liganding amino acid residue is presented in paretheses. The metal site geometry is also given for the wild-type protein for comparison.

1.2. Characterization of the Azurin Mutants. As been discussed before, the mass spectrometry confirmed the prepared mutants and also verified the formation of the novel disulfide bond itself. Furthermore, the constant ratio of the absorbance at 628 to 280 nm, compared to wild-type (not shown), indicated that the geometry of the copper site was not affected by the mutation, which also was confirmed later from the crystal structures (cf Table 6). The well-defined inflection point at 290 nm indicated that the mutations had not affected the localization of Trp48, a centrally positioned amino acid residue. This is true for all four mutants in this study and is also supported by crystal structures for K24R and D62C/K74C.

Evaluation of the thermostability for D62C/K74C by using DSC demonstrates that the introduced disulfide bond has an increased stability. The T_m value for the copper-containing mutant was increased by 3.7 °C. The result was based on extrapolation of DSC scans to an indefinite fast scan rate. The activation energy for the irreversible aggregation process was lower than that for the other mutants and the wild-type protein. Copper-containing D62C/K74C is therefore the only mutant in which the aggregation process is less favorable than that in the wild-type. The DSC scans on the zinc mutant showed a mainly reversible process and a suggested increase in thermostability of the same order as that in the Cu-D62C K74C mutant.

In this perspective, it is important to note that DSC measures the thermostability of the whole three-dimensional protein structure. Thermostability measured by spectrophotometry on the other hand monitors the changes in geometry around the copper site as a function of temperature. The accuracy of DSC is more significant since the method determines the thermostability of the global structure, and hence, our evaluation of the thermostability is focused on the results obtained from DSC. However, the spectrophotometric analysis of the thermal stability indicates a decrease in stability of the copper site for D23E/K128R and D23E/K128R/K24R. K24R and D62C/K74C show a stability in this area that is comparable to the wild-type protein.

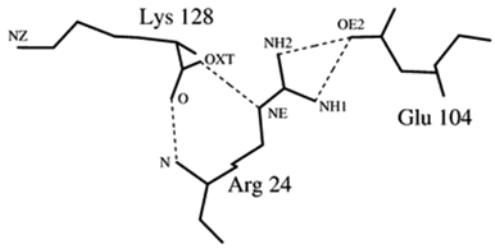

FIGURE 11: The novel hydrogen bond pattern formed by the mutated residue Arg24 and its neighbors Glu104 and Lys128.

Thermal denaturation of zinc azurin is reversible in the absence of oxygen (*10*). However, mutant D62C/K74C containing zinc in the metal site does not totally denaturate reversibly. The small DSC peak at the high melting temperature shows irreversibility, and this feature could be due to aggregation of the protein at elevated temperatures by unspecific cross-linking in or between monomers. The presence of two peaks in the DSC scan of this mutant is thus notable since its crystal structure shows that the mutant is almost identical to the structure from the copper-containing mutant D62C/K74C and the wild-type structure.

It could be further speculated that the zinc derivative of azurin with the novel disulfide bond has some degree of secondary structure in the unfolded state with a different stability compared to the rest of the protein at high temperature. There may be a number of explanations for this behavior, but we suggest that the most plausible explanation for the presence of two peaks in the DSC scan of the D62C/K74C mutant is the introduction of the disulfide bridge itself. This suggests among others an equilibrium between the folded state and at least two major conformations in the unfolded state. These conformations may occur because the engineered mutant has four discrete cysteines rather than two in the unfolded state, and it is outside the scope of this investigation to further analyze this situation.

2. Introduction of Electrostatic Interactions. The three mutants based on electrostatic interactions were all selected on the basis of stabilization of the "south part" of the protein. Regular atomic displacement factors, determined at ambient temperatures, indicated that there was a larger thermal motion in this area (Figure 2a). Mutant K24R was consequently selected to stabilize two loops closely located in separate β-strands. This amino acid substitution increased the stability by 1 °C for both copper and zinc derivates. The obtained X-ray structure of K24R supports the strategy behind the design of this mutant so that the interaction between the amino acid residues 24 and 104 really has become more favorable. Figure 11 shows a close-up view of the novel interactions between these residues. In particular, the engineered Arg24 contributes three new hydrogen bonds to the neighboring residues, 104 and 128. The improved thermostability, as judged from the atomic displacement factors (temperature factors) of K24R, indicates that this loop could be an important site for stabilization at elevated temperatures.

Mutant D23E/K128R was designed to stabilize the C-terminal end by an electrostatic interaction between the two amino acids. The stability of this mutant was decreased by 1 °C, and the aggregation process was more favorable in the mutant compared to the wild-type protein. Mutant D23E/K128R/K24R reflects stabilization of the C-terminus as well as the β-sheet. The thermostability for this mutant was comparable to D23E/K128R, and the aggregation process was also more favorable than that for wild-type azurin. It is possible that the positive effects from K24R compensated the steric effects and loss of native ion interactions in the triple mutant and hence the thermostability became the same as that for D23E/K128R. For the two mutants with a decreased stability, the gain of introduced interactions is obviously less compared to the loss of the native interactions.

Karshikoff and Ladenstein (*17*) give support to our strategy to improve thermostability of azurin by introducing electrostatic interactions. They argue that the driving force for enhancement of the thermotolerance of proteins from hyperthermophilic microorganisms is optimization of electrostatic interactions by an increase in the number of salt bridges. Introducing electrostatic interactions to increase the thermostability is not straightforward, however. It has been suggested by Elcock (*36*) that the effect of ion pairs for the thermostability of the protein is more significant at high temperatures. A complication concerning the electrostatic interactions occurs at lower temperatures, and it has been argued by Chakravarty and Varadarajanin in a recent theoretical analysis (*37*) that electrostatic interactions become more difficult to predict at lower temperatures due to desolvation penalties involved in burying ionic charges. It is clear that stabilization based on this type of interaction is a field for further investigations.

3. In Summary. Of the four selected mutants, only one, copper-containing D62C/K74C, showed a substantial increase in thermostability as determined by DSC, while the other three mutants did not affect the stability of azurin much. In addition, the crystal structures of mutants K24R and D62C/K74C supported the view that the increased thermostability is mostly due to the stabilization obtained in the protein from the engineered disulfide bond.

It was also found from the DSC scans of the zinc-containing disulfide mutant that the melting curve contains two distributions suggesting, among others, an equilibrium between the folded state and at least two predominant conformations in the unfolded state. This feature of a two-state transition has not been seen before, neither in the wild-type azurin protein and its metal derivatives nor in other single mutants of azurin. We have however found from the crystal structure solution that it is seemingly not an effect of a partial occupation of the zinc ion in the metal site, which may give rise to a similar melting curve (*6*).

The atomic displacement factors, determined at elevated temperatures, describe the molecular movements at higher temperatures. These were used to differentiate between conformational changes and regional melting in azurin that may take place in the crystalline state when the temperature is increased in steps over a defined range. The utilization of these factors in the design of the novel disulfide bond demonstrates, in our case, a useful tool in the research area of thermostability in proteins. This technique has in addition been used on thermostability measurements on ribonuclease A (unpublished work). Our thermostability study has also illustrated the use of regular atomic displacement factors determined at ambient temperatures, which presents an alternative approach in selecting mutants toward an increased thermostability.

ACKNOWLEDGMENT

We thank professor Tore Vänngård for helpful discussions and professor Hans Karlsson for the excellent experimental mass-spectrometric facilities put at our disposal.

REFERENCES

1. Nar, H., Messerschmidt, A., Huber, R., van der Kamp, M., and Canters, G. W. (1991) Crystal structure analysis of oxidized *Pseudomonas aeruginosa* azurin at pH 5.5 and pH 9.0. A pH-induced conformational transition involves a peptide bond flip, *J. Mol. Biol. 221*, 765−772.
2. Vijgenboom, E., Busch, J. E., and Canters, G. W. (1997) In vivo studies disprove an obligatory role of azurin in denitrification in *Pseudomonas aeruginosa* and show that azu expression is under control of rpoS and ANR, *Microbiology 143* (Part 9), 2853−2863.
3. Pascher, T., Chesick, J. P., Winkler, J. R., and Grey, H. B. (1996) Protein folding triggered by electron transfer, *Science 271*, 1558−1560.
4. Ökvist, M., Bonander, N., Sandberg, A., Karlsson, G. B., Krengel U., and Sjolin, L. (2001) Crystal Structure of the double mutant Cys3Ser/Ser100Pro from *Pseudomonas aeruginosa* to 2.0 Å resolution; its folding-unfolding energy and kinetics, *Biochim. Biophys. Acta 1596* (2), 336−345.
5. Carlsson, U., and Johnsson, B.-H. (1995) Folding of beta-sheet proteins, *Curr. Opin. Struct. Biol. 5*, 482−487.
6. Engseth, H. R., and McMillin, D. R. (1986) Studies of thermally induced denaturation of azurin and azurin derivatives by scanning calorimetry: evidence for copper selectivity, *Biochemistry 25*, 2448−2455.
7. Surewitcz, W. K., Szabo, A. G., and Matsch, H. H. (1987) Conformational properties of azurin in solution as determined from resolution-enhanced Fourier transform infrared spectra, *Eur. J. Biochem. 167*, 519−523.
8. LaRosa, C., Milardi, D., Grasso, D., Guzzi, M., and Sportelli, L. (1995) Thermodynamics of the thermal unfolding of azurin, *J. Phys. Chem. 99*, 14864−14870.
9. Guzzi, R., Sportelli, L., LaRosa, C., Milardi, D., Grasso, D., Verbeet, M. Ph., and Canters, G. W. (1999) A Spectroscopic and Calorimetric Investigation on the Thermal Stability of the Cys3Ala/Cys26Ala Azurin Mutant, *Biophys. J. 77*, 1052−1063.
10. Sandberg, A., Leckner, J., Shi, Y., Schwarz, F. P., and Karlsson, B. G. (2002) Effects of Metal Ligation and Oxygen on the Reversibility of the Thermal Denaturation of *Pseudomonas aeruginosa* Azurin, *Biochemistry 41*, 1060−1069.
11. Leckner, J., Bonander, N., Wittung-Stafshede, P., Malmström, B. G., and Karlsson, B. G. (1997a) The effect of the metal ion on the folding energetics of azurin: a comparison of the native, zinc a apoprotein, *Biochim. Biophys. Acta 1342*, 19−27.
12. Wittung, P., Källebring, B., and Malmström, B. G. (1994) The cupredoxin fold is found in the soluble Cu-A and CyoA domains of two terminal oxidases, *FEBS Lett. 349*, 286−288.
13. Leckner, J., Wittung, P., Bonander, N., Karlsson, B. G., and Malmström, B. G. (1997b) The effect of redox state on the folding free energy of azurin, *J. Biol. Inorg. Chem. 2*, 368−371.
14. Bonander, N., Leckner, J., Guo, H., Karlsson, G. B., and Sjolin, L. (2000) Crystal structure of disulphide deficient azurin mutant C3A/C26A.; How important is the S−S bond for folding and stability? *Eur. J. Biochem. 267*, 4511−4519.
15. Meyer, J., Clay, M. D., Johnson, M. K., Stubna, A., Munck, E., Higgins, C., and Wittung-Stafshede, P. (2002) A hyperthermophilic plant-type [2Fe-2S] ferredoxin from Aquifex aeolicus is stabilized by a disulfide bond, *Biochemistry 41* (9), 3096−3108.
16. Isupov, M. N., Fleming, T. M., Dalby, A. R., Crowhurst, G. S., Bourne, P. C., and Littlechild, J. A. (1999) Crystal structure of the glyceraldehyde-3-phosphate dehydrogenase from the hyperthermophilic archaeon *Sulfolobus solfataricus*, *J. Mol. Biol. 291* (3), 651−660.
17. Karshikoff, A., and Ladenstein, R. (2001) Ion pairs and the thermotolerance of proteins from hyperthermophiles: a "traffic rule" for hot roads, *Trends Biochem. Sci. 26* (9), 550−556.
18. Frauenfelder, H., Petsko, G. A., and Tsernoglov, D. (1979) Temperature-dependent X-ray diffraction as a probe of protein structural dynamics, *Nature (London) 280*, 558−563.
19. Petsko, G. A., and Ringe, P. (1984) Fluctuations in protein structure from X-ray diffraction, *Annu. Rev. Biophys. Bioeng. 13*, 331−371.
20. Fersht, A. R., and Serrano, L. (1993) Principles of protein stability derived from protein engineering experiments, *Curr. Opin. Struct. Biol. 3*, 75−83.
21. Sjolin, J., Langer, V., Alvarez-Rúa, C., Thanki, N., Ladner, J. E., and Gilliland, G. L. (2001) Probing the thermostability with X-ray crystallography; structure of ribonuclease S at elevated temperatures, manuscript in preparation.
22. Nar, H., Messerschmidt, A., Huber, R., van de Kamp, M., and Canters, G. W. (1992) Crystal structure of *Pseudomonas aeruginosa* apo-azurin at 1.85 Å resolution, *FEBS Lett. 306*, 119−124.
23. Karlsson, B. G., Pascher, T., Nordling, M., Arvidsson, R., H., A., and Lundberg, L. G. (1989) Expression of the blue copper protein azurin from *Pseudomonas aeruginosa* in *Escherichia coli*, *FEBS Lett. 246*, 211−217.
24. *Area Detector control and integration software*; SMART and SAINT, Siemens AXS Inc: Madison, WI, 1995.
25. DeLano, W. L., and Brünger, A. T. (1995) The direct rotation function: rotational Patterson correlation search applied to molecular replacement, *Acta Crystallogr. D51*, 740−748.
26. Brünger, A. T. (1997) Patterson correlations searches and refinement, in *Methods in Enzymology* (Carter, C. W., and Sweet, R. M., Eds.) Vol 276, part A, pp 558−580, Academic Press, Inc, London.
27. Brünger, A. T. (1992) *X-PLOR. Version 3.1. A system for X-ray crystallography and NMR*; Yale University, New Haven, CT.
28. Kirchhoff, W. H. (1993) *Exam: A Two-State Thermodynamic Analysis Program*, NIST Technology Note 1401, pp 1−103, National Institute of Standards and Technology, Rockville, MD.
29. Murshudov, G. N., Vagin, A. A., Lebedev, A., Wilson, K. S., and Dodson, E. J. (1999) Efficient anisotropic refinement of macromolecular structures using FFT, *Acta Crystallogr. D55*, 247−255.
30. Navaza, J. (1994) Amore − an Automated Package for Molecular Replacement, *Acta Crystallogr. D50*, 157−163.
31. Lamzin, V. S., and Wilson, K. S. (1993) Automated refinement of protein models, *Acta Crystallogr. D49*, 129−147.
32. Adams, P. D., Pannu, N. S., Read, R. J., and Brünger, A. T. (1997) Cross-validated maximum likelihood enhances crystallographic simulated annealing refinement, *Proc. Natl. Acad. Sci. U.S.A. 94*, 5018−5023.
33. Brünger, A. T., Adams, P. D., Clore, G. M., DeLano, W. L., Gros, P., Grosse-Kunstleve, R. W., Jiang, J. S., Kuszewski, J., Nilges, M., Pannu, N. S.,. Read, R. J,. Rice, L. M, Simonson T., and Warren, G. L. (1998) Crystallography & NMR system: A new software suite for macromolecular structure determination, *Acta Crystallogr. D54*, 905−921.
34. Jones, T. A., Zou, J. Y., Cowan S. W., and Kjeldgaard, M. (1991) Improved methods for binding protein models in electron density maps and the location of errors in these models, *Acta Crystallogr. A47*, 110−119.
35. Sanchez-Ruiz, J. M., Lopez-Lacomba, J. L., Cortijo, M., and Mateo, P. L. (1988) Differential scanning calorimetry of the thermal denaturation of Thermolysin, *Biochemistry 27*, 1648−1652.
36. Elcock, A. H. (1998) The stability of saltbridges at high temperatures: implications for hyperthermophilic proteins, *J. Mol. Biol. 284*, 489−502.
37. Chakravarty, S., and R. Varadarajan (2002) Elucidation of factors responsible for enhanced thermal stability of proteins: a structural genomics based study, *Biochemistry 41* (25), 8152−8161.

BI048926X